Available on CMS information server

CMS CR -2016/043

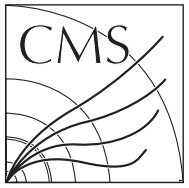

The Compact Muon Solenoid Experiment

Conference Report

Mailing address: CMS CERN, CH-1211 GENEVA 23, Switzerland

19 March 2016 (v2, 24 March 2016)

Pixel Sensors with slim edges and small pitches for the CMS upgrades for HL-LHC

Caterina Vernieri, Gino Bolla, Ryan Rivera, Lorenzo Uplegger, Irene Zoi for the CMS collaboration

Abstract

Planar n-in-n silicon detectors with small pitches and slim edges are being investigated for the innermost layers of tracking devices for the foreseen upgrades of the LHC. Sensor prototypes compatible with the CMS readout, fabricated by Sintef, were tested in the laboratory and with a 120 GeV/c proton beam at the Fermilab test beam facility before and after irradiation with up to 2x10^{15} n_{eq}/cm^2 fluence. Preliminary results of the data analysis are presented.

Presented at *VCI 2016 14th Vienna Conference on Instrumentation*

Pixel Sensors with slim edges and small pitches for the CMS upgrades for HL-LHC

Caterina Vernieri, Gino Bolla, Ryan Rivera, Lorenzo Uplegger, Irene Zoi for the CMS collaboration

Fermilab, Batavia, IL, 60510, USA

Abstract

Planar n-in-n silicon detectors with small pitches and slim edges are being investigated for the innermost layers of tracking devices for the foreseen upgrades of the LHC. Sensor prototypes compatible with the CMS readout, fabricated by Sintef, were tested in the laboratory and with a 120 GeV/c proton beam at the Fermilab test beam facility before and after irradiation with up to $2\text{x}10^{15}$ n_{eq}/cm^2 fluence. Preliminary results of the data analysis are presented.

Keywords: Tracking detectors, Planar silicon pixel sensors, Radiation hardness, CMS, LHC upgrade

1. Introduction

The CMS collaboration has an ongoing R&D plan to develop a new tracking system able to operate at and above the design luminosity of the HL-LHC [1]. In particular the pixel detector will be replaced with a new one (Phase−II−Pixel) to maintain a high tracking and b-jet identification efficiency at luminosities up to $5{\cdot}10^{34}$ $cm^{-2}s^{-1}$.

The Phase−II−Pixel will extend the η coverage from the present η =2.5 to η =4, will have smaller pixels and will have to withstand one order of magnitude higher radiation damage. The foreseen integrated luminosity of 3000 fb^{-1} together with the high particle rates demand sensors with higher granularity and a sensor design with limited dead area surrounding the active pixel array.

The prototype sensors characterized in this document were fabricated by Sintef [2] in the unused area of the wafers used for the Phase-I CMS pixel upgrade production. The fabrication process is symmetric and uses five masks on each side, n-in-n double sided technology with guard-rings on the p-side [3]. All prototypes have an active area of 7.8x8 mm^2, a standard periphery of 1.2 mm width and are implemented on a substrate with a thickness of 300 µm. The prototype sensors are bump-bonded to a single PSI46Digv2.1 Read Out Chip (ROC) [4]. This approach has the advantage of relying on an established production processes to test new key features for the upgraded tracking system.

2. Small Pitch

To investigate smaller pixels, the prototype sensor active area is split in three regions, each one with a different pitch but all keeping the same pixel area (Fig. 1): a control region with the standard 150x100 μm^2 pixel shape (20 rows and 52 columns), a second region with 300x50 μm^2 pixel shape (30 rows and 26 columns) and a third region with 600x25 μm^2 pixel shape (60 rows and 13 columns). For all three regions the p-stops in the inter pixel areas are implemented with a common grid implantation. In order to maintain the same bump-bonding pattern on the sensor as on the ROC, the pixel area has to remain the same and the metallization has to be implemented with small metal lines routing the pixel signal to the input pads of the front-end ASIC. The cross-over of these lines with the underlying pixels has the potential to introduce a spurious cross-talk that can result in undesired charge sharing.

The devices are first characterized in terms of DC performance at the probe station. The depletion voltage from the capacitance-voltage (CV) characteristic is 75 V, while the breakdown voltage is well above the depletion voltage. The total leakage current is less than 20 nA/cm^{-2} .

The hybridized detectors were calibrated with the data acquisition system to the minimum stable threshold. The three regions have a different capacitive load for the front end amplifier resulting in different noise level. The 600x25 μm^2 pixels have a noise level of 240 e^-, which is about twice the noise level measured on the regular 150x100 μm^2 pixels. The thresholds were tuned to 2400 e^- for all three zones, and the gain curves were recorded on a pixel by pixel basis.

The sensors were tested with 120 GeV/c protons at the Fermilab Test Beam Facility (FTBF) in June and December 2015. FTBF is equipped with a silicon pixel telescope, which is permanently installed and available to users [5]. The telescope consists of eight planes of planar CMS pixel detectors, four measuring with higher precision the *y*-coordinate and the other four the *x*-coordinate. In order to exploit the improvement in the spatial resolution, that results from charge sharing between adjacent pixels, the planes are tilted by 25° with respect to the beam axis. Up to three Devices Under Test (DUTs) were placed in the middle of the telescope. Only tracks from events with a single hit in each of the telescope planes were used in the anal-

*Corresponding author

Email address: cvernier@fnal.gov (Caterina Vernieri, Gino Bolla, Ryan Rivera, Lorenzo Uplegger, Irene Zoi for the CMS collaboration)

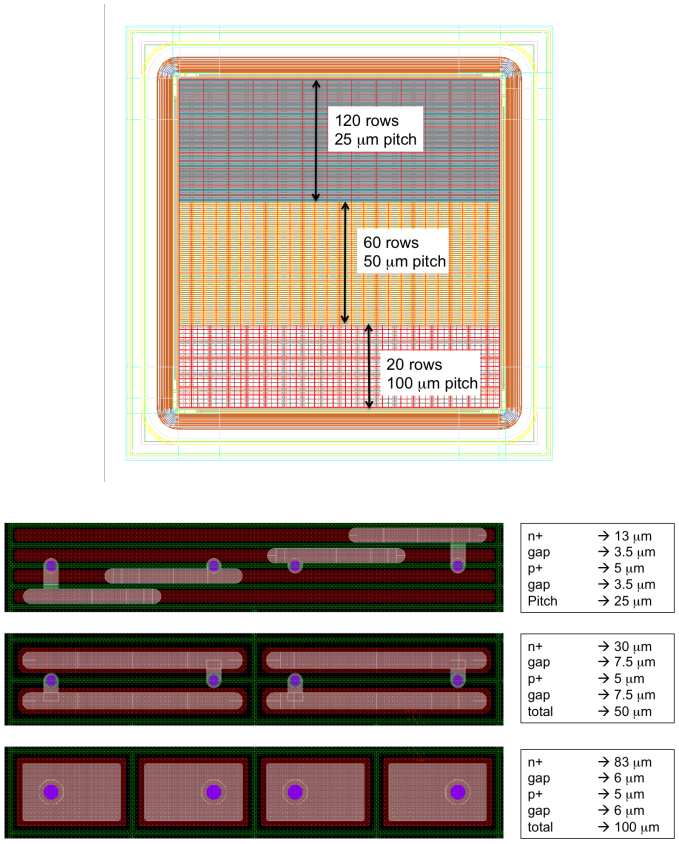

Figure 1: Drawings of the pixel sensor prototype with smaller pitch. Maintained the same pixel area 100x150μm^2 that is implemented in the Phase-I design (top). Single ROC sensor split in three regions with three different pitches (bottom).

ysis. The precision obtained at the plane of the DUT is, on average, 8 μm in both spatial directions.

The efficiency is computed by requiring that either the pixel the track points to or one of its neighboring pixels has a hit, to take into account the error on the track projection. The measured efficiency is > 99.5% independent of the pixel geometries. The missing 0.5% is likely to be attributed to timing problems in the synchronization between the 40 MHz ROC clock and the 52 MHz beam clock.

The cluster size increases as the pixel pitch decreases as shown in Fig. 2, resulting in a negligible number of single pixel clusters and an unexpected number of size three and four clusters for the smallest pitch (25 μm). These large clusters are probably due to the cross talk between pixels induced by the metallization pattern, as described in Fig. 1. The collected cluster charge is the same in the three regions, showing a Landau peak of 24000 e− as expected given the devices' thickness.

The spatial resolution is estimated using the residuals calculated as the difference between the measured impact point and the predicted impact point from the track reconstruction. The measured impact point is computed as the center of mass of the cluster. In Fig. 3 the residuals for each region are shown. The resolution is then quantified using the sigma of a Gaussian fit to the residuals distribution. The measured resolution is 27.7 μm for 150x100 μm^2, 12 μm for 300x50 μm^2 and about 9.9 μm

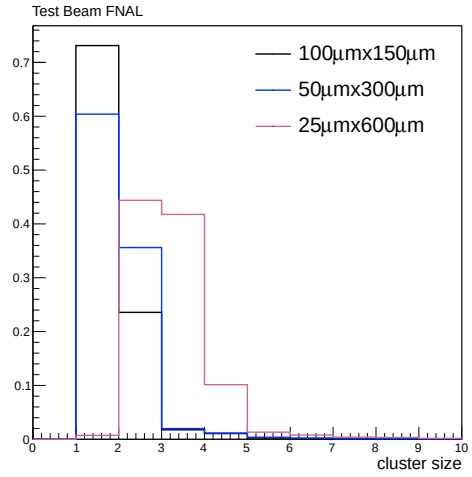

Figure 2: Small Pitch prototype operated at V=120 V at FTBF. Cluster size measurement is compared between three different regions of the sensor with different pitch (150x100 μm^2, 300x50 μm^2 and 600x25 μm^2).

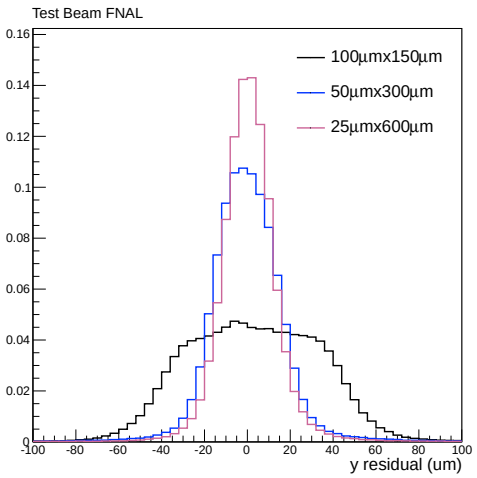

Figure 3: Small Pitch prototype operated at V=120 V at FTBF. Resolution measurement for inclusive cluster size for the three different regions of the sensor with different pitch (150x100 μm^2, 300x50 μm^2 and 600x25 μm^2). The short pitch pixel direction is considered (y-axis).

for 600x25 μm^2, if all cluster sizes are considered. Taking into account the telescope resolution of 8 μm, the hit resolution is 5.8 μm for the 25 μm pitch.

For the smallest pitch region, data have have been analyzed with a different approach and with a tighter track selection[1]. Residuals are computed using the charge asymmetry method to improve the measurement of the impact point [6]. The asymmetry is defined for size-two clusters only as the difference of the charge in the two pixels divided by the cluster's total charge:

$$\eta = \frac{Q_{down} - Q_{up}}{Q_{down} + Q_{up}} \quad (1)$$

where "up" and "down" are referring to the y-direction along

[1]Tracks are required to have two-pixel clusters in each telescope plane.

the short pitch.
The resulting function from the linear fit to the asymmetry profile is then used to extract the residual. The resolution, using the asymmetry correction is about 7.2 μm for all pitches. Taking into account the telescope resolution[2] of 6.2 μm, the corrected hit resolution for size two clusters is 3.6 μm.

The prototypes were irradiated at the CERN PS irradiation facility [7] at two different fluences corresponding to 2 and 6x10^{15} n$_{eq}$/cm^2. The sensors irradiated at the highest dose were used to study the breakdown behavior, which is not presented here. The charge collection was studied for the lower fluence only, as the ROC delivers only binary information after irradiation to 250 MRad [8]. After irradiation the sensors were stored and operated at -20 °C at FTBF to avoid annealing and to minimize the leakage current. The prototypes were calibrated under these conditions, and the minimum stable threshold achieved was 3500 e$^-$. Such an increase in threshold is likely a consequence of the inhomogeneity of the integrated fluence over the detector area, due to non-optimal alignment of the devices with respect to the beam during the radiation exposure. We estimate a factor of 3-4 different fluence for opposite corners of the devices.

The effects of the radiation on charge collection efficiency and on cluster size are shown in Fig. 4 and Fig. 5 respectively, where a comparison with the performance before irradiation can be made. The data before irradiation have been also analyzed with an artificial offline threshold of 3500 e$^-$ (instead of the 2400 e$^-$ that was used during data taking) in order to facilitate the comparison. The collected charge is decreased by radiation effects from 24000 e$^-$ to 10000 e$^-$, which is compatible with literature [9], with a direct consequence on the cluster size, which is further amplified by the high threshold used for the data taking.

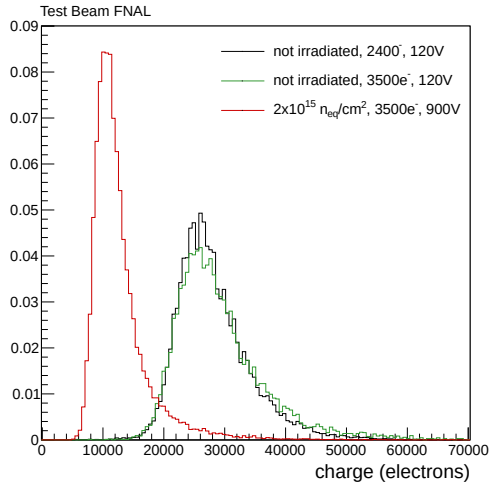

Figure 4: Small Pitch prototype focusing on the region with 600x25 μm^2 pitch. Cluster charge measurement for size-two clusters. The prototype has been irradiated at 2x10^{15} n$_{eq}$/cm^2. The irradiated device is operated at V=900 V and -20 °C and compared to the not irradiated device operated at V=120 V at FTBF.

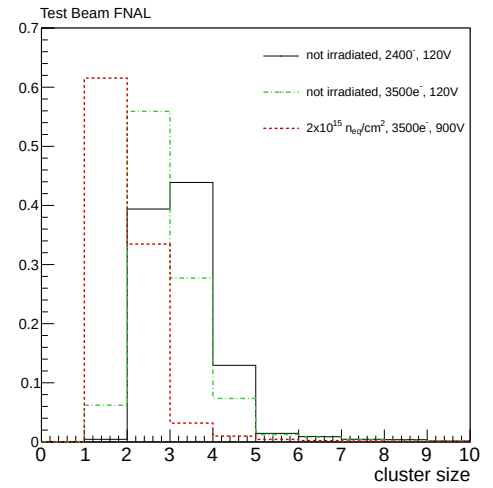

Figure 5: Small Pitch prototype focusing on the region with 600x25 μm^2 pitch. Cluster size measurement performed at FTBF. The prototype has been irradiated at 2x10^{15} n$_{eq}$/cm^2. The irradiated device is operated at V=900 V and -20 °C and compared to the not irradiated operated at V=120 V.

3. Slim Edge

The Slim Edge prototypes are regular sensors where one of the four edges has been reduced in width with the goal of minimizing the dead region between the end of the active area (pixel array) and the physical edge of the sensor (dicing line) in order to achieve better acceptance and hermeticity. Such an approach has already been implemented by ATLAS collaboration for IBL [10].

The pixel array (active area) normally ends at 1150 μm from the dicing edge (bottom edge of Fig. 6). In these prototypes this distance is reduced to 210 μm corresponding to a net reduction of 950 μm (right edge of Fig. 6). In Figure 6 it is also visible that the last column of pixels on the right hand side overlap partially with the first large guard-ring (GR1) implemented on the opposite side of the substrate (p-side). The connection of this first guard-ring to the backside potential can be implemented and removed at will to measure the impact on the performance.

The devices are first characterized in terms of DC performance at the probe station. The depletion voltage is measured from the CV curve to be about 80 V, while breakdown voltage is well above the depletion voltage. The current-voltage (IV) characteristic post dicing and bump-bonding shows an additional component to the leakage current that is visible starting at about 180 V and has a linear behavior with respect to the voltage applied thereafter with a slope of 2 μA per 100 V. The onset voltage of this effect is lowered to 140 V if GR1 is connected to the backside potential pointing to the source of the current being on the device edge.

Sensors were characterized at FTBF with 120 GeV/c protons with a particular emphasis on the behavior of the external columns. The performance of the last column of pixels (Slim Edge) in term of efficiency and charge collection is compared

[2] A tighter track selection is applied for the asymmetry computation.

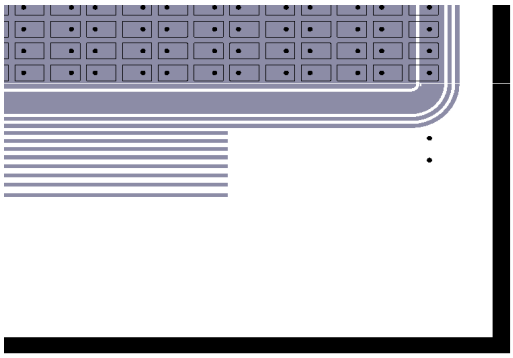

Figure 6: Drawing of the pixel sensor prototype with reduced inactive area. The picture shows the bottom right corner of the device where the standard periphery is implemented at the bottom and the novel periphery with reduced number of guard-rings is implemented on the right edge. The length of the inactive region is reduced from 1150 µm to 210 µm.

with the first column of pixels (Standard Edge) to understand the impact of the novel periphery. In Fig. 7 we compare the efficiency between the standard and the slim edge, and the efficiency of the central column is reported as reference. The loss of efficiency on the edges with respect to the central region is due to the error on the track extrapolation. The result of this comparison is that standard and slim edge behave similarly. The efficiency is slightly worse for the slim edge, but this effect is limited to the last 15 µm, to be compared to the 950 µm gained by reducing the dead area (≈ 6 pixels). A similar comparison is shown in Fig. 8 for the charge collection efficiency, which shows a degradation of the performance of the slim edge in half of the pixels (75 µm). Fig. 8 also provides a performance comparison between when there is a connection to GR1 and when there is not. The connection to GR1 is clearly beneficial in terms of charge collection efficiency, but as stated earlier, it increases the leakage current. Post-irradiation results are not available for the slim edge prototype.

4. Conclusions

R&D for the CMS HL-LHC upgrade is ongoing to cope with the challenges associated with the foreseen instantaneous and integrated luminosities. Different technologies and prototype are being investigated in simulation and submissions are under way. Here the characterization of n-in-n prototypes silicon detectors has been presented. Sensors with small pitch and slim edge have been bump-bonded to the CMS ROC, characterized in the laboratory and tested with 120 GeV/c protons. Small Pitch sensors are found to be fully efficient independent of the pitch and with resolution as good as 3.6 µm. After irradiation they are operable and fully efficient up to $2\text{x}10^{15}$ $\text{n}_{eq}/\text{cm}^2$ fluence. Slim Edge sensors are fully efficient up to 300 µm from the diced edge, and charge collection efficiency is reduced only for half of the last pixel column.

[1] CMS Collaboration, CERN-LHCC-2015-010 ; LHCC-P-008, (2015).
[2] https://www.sintef.no/en/
[3] G. Bolla et al., Nucl. Instrum. Meth. A **501**, 160-163 (2003).
[4] H. C. Kaestli et al., Nucl. Instrum. Meth. A **565**, 188 (2006) doi:10.1016/j.nima.2006.05.038 [physics/0511166].

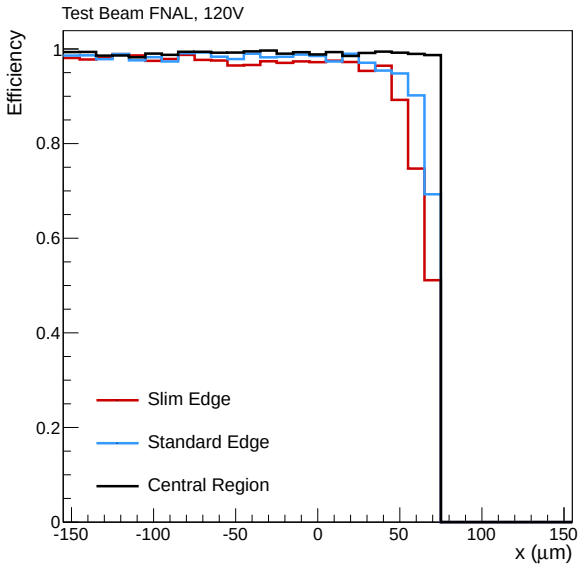

Figure 7: Slim Edge sensor prototype operated at V=120 V at FTBF. The efficiency is shown as function of the position on the device in the long pixel direction (*x*-axis). It is compared between three different regions of the sensor. Central columns are shown in black and compared to the external left (blue, regular edge) and external right (red, slim edge) columns.

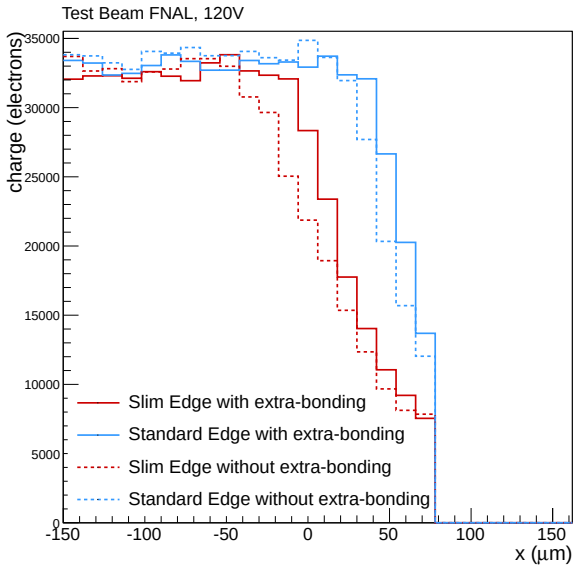

Figure 8: Slim Edge sensor prototype operated at V=120 V at FTBF. Charge collection measurement is shown as function of the position on the device in the long pixel direction (*x*-axis). It is compared between two different regions of the sensor, if the extra-bonding is present (solid) or not (dashed). External left columns are shown in blue and compared to the external right (red, slim edge) columns.

[5] S. Kwan et al., Nucl. Instrum. Meth. A **811**, 162 (2016) doi:10.1016/j.nima.2015.12.003.
[6] L. Moroni, L. Uplegger et al., Journal of Instrumentation, **8** 06 (2013).
[7] https://irradiation.web.cern.ch/irradiation/
[8] J. Hoss, CMS-CR-2015-253 (2015).
[9] M.Moll (on behalf of RD50 collaboration), World Scientific, pp 101-110,

(2010) ISBN: 978-981-4307-51-2/3.
[10] Atlas Collaboration, CERN-LHCC-2010-013 ; ATLAS-TDR-19 (2010).